

GT2011-46626

## MEASUREMENT OF VOLATILE PARTICULATE MATTER EMISSIONS FROM AIRCRAFT ENGINES USING A SIMULATED PLUME AGING SYSTEM

Jay Peck\*, Michael T. Timko, Zhenhong Yu, Hsi-Wu Wong, Scott C. Herndon,  
Paul E. Yelvington†, and Richard C. Miake-Lye  
Aerodyne Research, Inc., Billerica, Massachusetts

Changlie Wey  
ASRC Aerospace Corp., Cleveland, Ohio

Edward L. Winstead  
GATS, Inc., Newport News, Virginia

Luke D. Ziemba, and Bruce E. Anderson  
NASA Langley Research Center, Hampton, Virginia

### ABSTRACT

Aircraft exhaust contains nonvolatile (soot) particulate matter (PM), trace gas pollutants, and volatile PM precursor material. Nonvolatile soot particles are predominantly present at the engine exit plane, but volatile PM precursors form new particles or add mass to the existing ones as the exhaust is diluted and cooled. Accurately characterizing the volatile PM mass, number, and size distribution is challenging due to this evolving nature and the impact of local ambient conditions on the gas-to-particle conversion processes. To accurately and consistently measure the aircraft PM emissions, a dilution and aging sampling system that can condense volatile precursors to particle phase to simulate atmospheric evolution of aircraft engine exhaust has been developed. In this paper, field demonstration of its operation is described. The dilution/aging probe system was tested using both a combustor rig and on-wing CFM56-7 engines. During the combustor rig testing at NASA Glenn Research Center, the dilution/aging probe supported formation of both nucleation/growth mode particles and soot coatings. The results showed that by increasing residence time, the nucleation particles become larger in size, increase in total mass, and decrease in number. During the on-wing CFM56-7 engine testing at Chicago Midway Airport, the dilution/aging probe was able to form soot coatings as well as nucleation mode particles, unlike conventional 1-m probe engine measurements.

*The number concentration of nucleation particles depended on sample fraction and relative humidity of the dilution air. The performance of the instrument is analyzed and explained using computational microphysics simulations.*

### INTRODUCTION

Particulate matter (PM) emissions from aircraft engines are getting increasing attention due to their proven and suspected impact on global climate change, local air quality, and human health [1–5]. Although accurate and consistent measurements are required to better understand their impact, and possibly improve on current practices, characterizing the volatile PM mass, number, and size distribution is a technical challenge [6–10]. Aircraft engines emit both nonvolatile (soot) particles and volatile PM precursor species. PM emissions evolve from being dominated almost exclusively by soot at the engine exit plane to a complex mixture of soot, sulfates, and condensed organics as the exhaust stream cools and mixes with ambient air [10–20]. The evolving nature of the PM matrix, as condensable gases both form new particles and add mass to existing particles, complicates the measurement as to where and how to sample the particles to capture the volatile components reproducibly and systematically.

In addition to being a “moving target”, volatile PM is poorly transmitted through engine sampling systems to the characterization equipment. Gas-to-wall loss may dominate the desired gas-to-particle conversion under some conditions. Also, the volatile particles are typically much smaller than 100 nm, and the trans-

\*Corresponding author: jpeck@aerodyne.com

†Present address: Mainstream Engineering Corp, Rockledge, Florida

mission of small particles through the sampling system is poor. Despite significant advancement in the measurement instrumentation to provide the required measurement capabilities, the difficulty to transport the volatile PM to the instruments still remains. During research activities, a number of studies have focused on sampling the particulate emissions at downstream locations in the exhaust plume [21–24]. While this practice has provided useful information, downstream sampling depends on favorable winds, can be influenced by ambient conditions [12,25], and is incompatible with current certification practice. Standardized tests would be nearly impossible when ambient conditions play a large role in the measurement results, not to mention the complexity of logistical issues associated with the need for a large test area. Thus, while the volatile PM emission is an important research subject for environmental effects and possible regulatory reasons, making consistent and reliable measurements from aircraft engines still remains to be addressed.

To reproducibly measure the PM emissions from aircraft engines regardless of fluctuations of the local ambient conditions, we have designed, built, and tested the Simulated Aircraft Exhaust Plume Aging (SAEPA) probe system. The SAEPA probe is an extractive sampling probe with a dilution and aging capability that allows volatile PM to form consistently and reliably, and simulates microphysical gas-to-particle conversion that approximates atmospheric processing during mixing and dilution in the atmosphere. The exhaust sample is extracted at the engine-exit plane, but the sample is diluted and aged, so that volatile precursor’s behavior is similar to sampling at several tens of meters downstream of the engine. It minimizes gas-to-wall and particle-to-wall losses, is independent of ambient conditions, does not depend on favorable winds, and is compatible with current certification practice. By controlling the relevant dilution parameters, standardized measurements can be defined and consistent measurements can be obtained without concern for variations in ambient conditions. The instrument was experimentally tested with two emissions sources: a combustor test rig at NASA Glenn Research Center and on-wing CFM56-7 engines at Chicago Midway Airport. In this paper, the field deployment results are presented, and the results are explained and discussed using microphysical simulations.

## METHODS

### Aerodyne SAEPA Probe System

Aerodyne Research Inc. (ARI) developed the SAEPA probe through rigorous design case studies, modeling, and flow characterization with non-reacting flows. The probe extracts the exhaust gas from the engine exit plane (or immediately downstream of the engine), and transfers the sample through a heated ( $> 150^{\circ}\text{C}$ ) stainless steel tube to a dilution and aging chamber. Transferring the sample through a heated tube is required to prevent microphysical reactions as well as thermophoretic loss of soot particles [25–28]. The dilution/aging chamber is a cylinder with a diameter of 10 cm and a length of 1.8 m. The exhaust sample is injected into the chamber at the centerline, and the dilution gas (either nitrogen or  $\text{CO}_2$ -free air) is introduced as a sheath co-flow. This flow scheme is illustrated in Figure 1, which shows the inlet region of the dilution/aging chamber. We chose to inject the exhaust as a turbulent jet into a laminar dilution co-flow because this

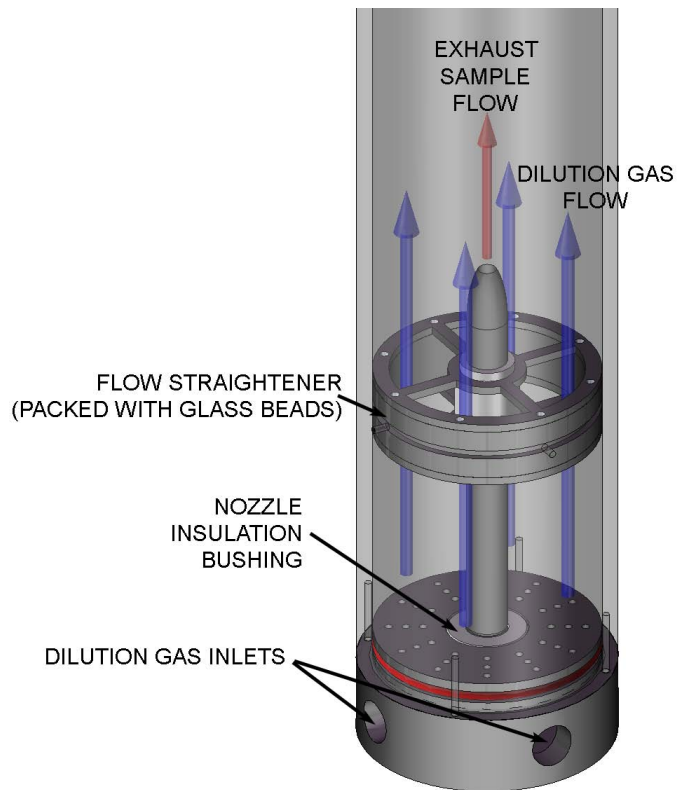


Figure 1. Schematic of the inlet region of the plume dilution/aging chamber

configuration 1) mimics the jet engine plume traveling through the ambient air, 2) minimizes the effect of the chamber wall during the critical microphysical processes, and 3) is a well defined flow [29, 30]. The dilution gas is conditioned to achieve the desired temperature and relative humidity prior to introduction to the chamber, and it goes through a packed-bed flow straightener to become a uniform plug-flow. Within the chamber, the exhaust sample and dilution gas mix in a well-defined manner. We plan to describe detailed theoretical underpinnings of the chamber design, flow/mixing characterization, detailed laboratory evaluation, and microphysical simulations in a separate publication.

### Field Tests

The SAEPA system was deployed to two venues for field testing. First, it was deployed to the CE-5 combustor test cell at NASA Glenn Research Center (GRC), and tested with a lean-direct inject (LDI) combustor rig [35]. The CE-5 combustor rig is a 76 mm square flame-tube, featuring an array of 25 or 36 simplex fuel nozzles that atomize fuel into fine droplets and mix with air quickly to reduce  $\text{NO}_x$  production. The CE-5 combustor rig has some similarities to a full engine, but also some important differences. The most important difference is that exhaust gas samples are extracted directly from the high-pressure/high-temperature combustor rig. We placed significant effort into understanding how to interface the dilution/aging chamber with the combustor rig. The burner exhaust sample was extracted with a probe that is embedded inside the flame tube approximately 20 cm away from the fuel injector plane, went through a 0.5 mm critical orifice to reduce the pressure and through a shut-off valve

Table 1. Experimental setup for field deployments

Parameter	NASA GRC CE-5	Chicago Midway Airport
Emissions source	LDI combustor rig	four on-wing CFM56-7 engines
Fuel	JP8	JetA
Probe inlet pressure	>1 atm (supplied by combustor pressure)	<1 atm (sample extracted via a pump)
Sampling line <sup>a</sup>	3 m long & 12.7 mm o.d.	20 m long & 12.7 mm o.d.
Transfer line <sup>b</sup>	15 m long & 12.7 mm o.d.	2 m long & 9.5 mm o.d.

<sup>a</sup> Sampling line refers to the tube that delivers the exhaust sample from the 1-m probe to the dilution/aging chamber

<sup>b</sup> Transfer line refers to the tube that delivers the processed sample from the dilution/aging chamber to characterization equipment

Table 2. Specification of the characterization instruments

Instrument	Parameter measured	Units reported	Detection range	Time resolution	Reference
ARI C-ToF AMS	size-resolved particle mass and composition	$\mu\text{g}/\text{m}^3$	80 – 1000 nm	~10 sec.	Jayne <i>et al.</i> [31]
Thermo Electron MAAP 5012	black carbon soot mass	$\mu\text{g}/\text{m}^3$	$>5 \mu\text{g}/\text{m}^3$	~1.5 sec.	Petzold and Schönlinner [32]
TSI CPC 3022	number concentration	$\#/ \text{cm}^3$	0 – $10^7$ (>7 nm)	1 sec.	Sem [33]
TSI CPC 3775	number concentration	$\#/ \text{cm}^3$	0 – $10^7$ (>4 nm)	1 sec.	Sem [33]
TSI EEPS 3090	size-resolved number concentration ( $dN/d\log D_p$ )	$\#/ \text{cm}^3$	6 nm – 500 nm	1 sec.	Hagen <i>et al.</i> [34]
LI-COR LI-840	carbon dioxide (CO <sub>2</sub> )	ppm	2 – 10,000 ppm	1 sec.	

that can be remotely operated. Then, the sample was transferred to the dilution/aging chamber via a 3 m long, 12.7 mm o.d. section of stainless steel tube that was temperature-controlled to a wall temperature of 150 °C (“sampling line”). Downstream of the chamber, approximately 15 m long, 12.7 mm o.d. stainless steel tube kept at room temperature was used to deliver the processed sample to the instruments (“transfer line”).

The second venue was Chicago Midway Airport (MDW), and the SAEPA probe was tested using in-service, on-wing CFM56-7 aircraft engines as part of a more comprehensive measurement activity (subsequently referred to as MDW-10). MDW-10 consisted of sampling exhaust from four CFM56-7 engines operating near idle conditions. Exhaust gas samples were extracted at 1 m from the engine exit using a 1.5 mm i.d. sample probe (no tip dilution), and transported to the dilution/aging chamber via ~20 m of heated (150 °C) sampling line. Due to airport logistics, 20 m was the closest that we could position the instrument trailer to the test engine. The dilution/aging chamber was located in the trailer with a suite of characterization instruments, so the final transfer line between the chamber and the instruments was ~2 m. Table 1 summarizes the experimental setups for the two test venues.

A suite of characterization equipment supported the SAEPA probe during field deployments. Specifically, a condensation par-

ticle counter (CPC, either 3022 or 3775, TSI Inc., Shoreview, MN) was used to monitor particle number density, and an engine exhaust particle sizer (EEPS 3090, TSI Inc.) was used to measure particle size distribution. The EEPS sorts particles into 16 size bins and measures number density in each of these bins using electrometers operating at 1-Hz sampling frequency. The EEPS and kindred instruments that use a similar operating principle have been described in the literature [36–38], including their application to aircraft exhaust characterization [34]. To measure particle-phase organic mass, an aerosol mass spectrometer (C-ToF AMS, Aerodyne Research, Inc., Billerica, MA) was employed [31]. A non-dispersive infrared (NDIR) CO<sub>2</sub> analyzer (LI-840, LI-COR BioSciences, Lincoln, NE) was used to monitor CO<sub>2</sub> concentrations to determine the exhaust sample fraction in the processed gas. To compare with conventional probe technologies, a conventional particle probe with a CPC and EEPS was used during the CE-5 testing [10]. We also used a thermo-denuder and a CPC connected to the SAEPA probe in the CE-5 testing [14]. A thermo-denuder is a device that heats the aerosol particles to vaporize and remove volatile compounds. Comparison of thermo-denuded and non-denuded samples identifies the relative contributions of non-volatile and volatile PM. During the MDW-10 campaign, a 1-m particle probe with a multi-angle absorption photometer (MAAP,

Thermo Electron Corp., Waltham, MA) was used to obtain total black carbon mass [32]. In addition, the CFM56-7 engine is one of the most studied engine classes in the commercial fleet, and we have extensive performance data that can be used in comparing with the SAEPA probe measurements [15, 39]. Table 2 lists detailed specifications of the instruments used.

## Microphysical Simulation Code

A microphysical simulation code developed by Wong *et al.* [25] was used to explain the field test results and to better understand the physical meaning of the results. The code uses a 1-D microphysical model to track the time evolution of gaseous and PM species, specifically by evaluating the production or loss by chemical reactions, dilution and mixing, microphysical processes, and particle loss to the sampling line. The microphysical simulation code has been used to provide qualitative information to describe the particle microphysics in the aircraft exhaust plume. However, it has several limitations; most significantly, the current version does not include organic hydrocarbon microphysics. Hydrocarbon species in the exhaust plume are known to participate and generally enhance the microphysical processes [40–43], but the effects need to be studied further before they can be included in the model. For the simulations of field deployments, while aircraft soot emissions typically exhibit a log-normal distribution, we approximated the soot particles as having a monodisperse diameter of 16 nm and a number concentration of  $9.7 \times 10^6 \text{ cm}^{-3}$  to avoid excessive computational burden. This diameter and concentration have equivalent surface area to typical polydisperse soot particles obtained from an aircraft engine [15]. In addition, the exact composition of the combustor exhaust was not known, so the composition of typical aircraft engine exhaust at idle power was calculated using GasTurb [44] and used instead.  $\text{SO}_3$  concentration was estimated separately using a fuel sulfur content of 400 ppm and 1% conversion from  $\text{SO}_2$  to  $\text{SO}_3$ . Although the simulation results may not represent the experimental results quantitatively, they can still capture the qualitative behavior of the experimental data [45].

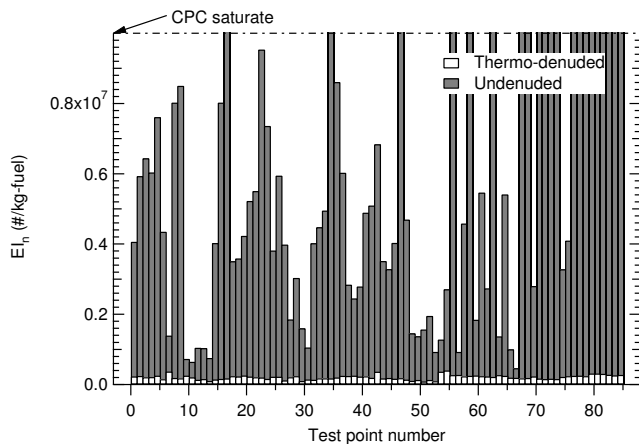


Figure 2. Comparison of the particle number concentrations between the thermally denuded and undenuded samples through the SAEPA probe.

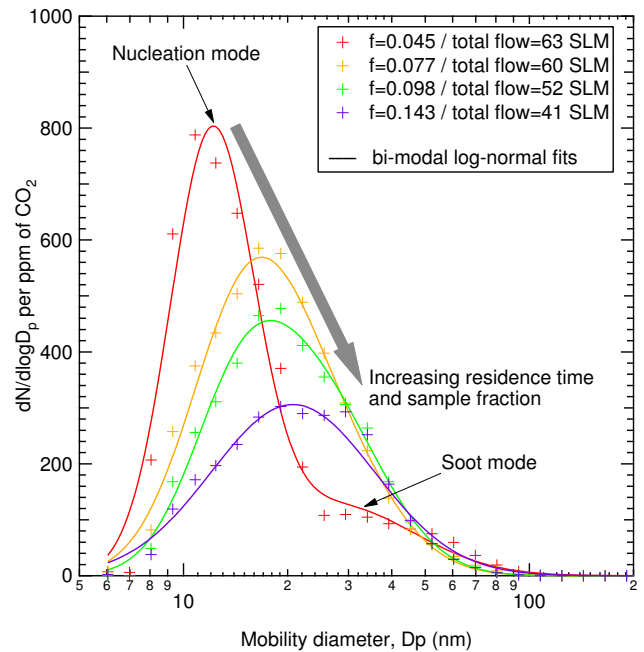


Figure 3. Particle size distribution (EEPS) obtained using the dilution/aging chamber during the CE-5 combustor rig tests.

## RESULTS AND DISCUSSION

### Combustor Rig Test

The combustor rig tests clearly established that the SAEPA probe supports gas-to-particle conversion. Using the SAEPA probe, the thermally denuded sample showed similar number densities as the conventional particle probe, but the undenuded sample registered a few orders of magnitude higher number densities, suggesting that many volatile nucleation mode particles are formed in the dilution/aging chamber. Figure 2 shows the comparison of number-based emissions index,  $EI_n$  (number of particles per kilogram of fuel burnt), of the thermally denuded and the undenuded samples from the SAEPA probe. The exact ratio between the concentrations of the denuded and the undenuded samples varied depending on the dilution levels and the residence time.

Figure 3 shows the particle size distribution obtained using the EEPS. Sampling through the SAEPA system, the EEPS typically showed two distinct peaks, one around 15 nm and the other around 35 nm, whereas the conventional particle probe displayed only one peak around 35 nm. We assign the 15 nm peak to nucleation mode PM formed by gas-to-particle conversion, and the 35 nm peak to soot. For this measurement, the combustor inlet temperature was 500 K, exit temperature was 1380 K, and the combustor pressure was 1 MPa. JP8 fuel was burned at the overall equivalence ratio of 0.42. Figure 3 shows that the particle size distribution changes in response to sample fraction ( $f$ ) and total flow rate (sample + dilution), and the number concentration was corrected by the  $\text{CO}_2$  level to eliminate the first-order effect of dilution. The differences are attributed to microphysics. Flow residence time in the dilution/aging chamber varies inversely with the total flow rate, so higher total flow rates correspond to shorter residence times. During the CE-5 testing, the exhaust sample flow rate was nearly constant as it was supplied by combustor pressure and through a critical orifice. Therefore, the sample fraction could only be adjusted by varying the dilution flow rate, so the

sample fraction and the residence time were coupled. Figure 3 indicates that the nucleation mode of volatile PM grows in size from having a peak at approximately 10-15 nm to peaking in the 15-20 nm range as the sample fraction and/or residence time is increased. The soot mode is apparent at low sample fraction and/or residence time, but becomes buried under the nucleation mode as the nucleation mode grows in size.

The data in Figure 3 are representative of a much larger data set consisting of many hundreds of individual data points since the EEPS provided size distribution at every second. To analyze the data in more detail, we fitted the particle size distribution to a bi-modal log-normal distribution to capture both the soot and nucleation modes:

$$\frac{dN/d\log D_p}{C_{CO_2}} = a_1 \exp \left[ - \left( \frac{\log \left( \frac{D_p}{a_2} \right)}{a_3} \right)^2 \right] + b_1 \exp \left[ - \left( \frac{\log \left( \frac{D_p}{b_2} \right)}{b_3} \right)^2 \right]$$

Here,  $D_p$  is the mobility diameter of the particles [nm], and  $N$  is the number concentration of the particles [#/ $\text{cm}^3$ ], and  $C_{CO_2}$  is the measured  $CO_2$  concentration [ppm]. The first term represents nucleation mode particles, and the second term corresponds to the soot mode particles. From our experience during other engine tests and from our evaluation of the CE-5 data, we realized that the  $CO_2$ -normalized soot mode does not vary much in size and magnitude with respect to the dilution level. Therefore, the soot mode parameters were determined by fitting it for a low sample fraction case, where the soot mode was distinctly visible. We then fixed  $b_1$ ,  $b_2$ , and  $b_3$  at  $100 \text{ (cm}^3 \text{ ppm)}^{-1}$ , 35 nm, and 0.55, respectively. With these parameters fixed, the remaining nucleation mode parameters were regressed for each separate particle size distribution. Figure 4 shows the best-fit geometric mean diameter (GMD) of the nucleation mode ( $a_2$ ) plotted versus the sample fraction. The marker color represents the magnitude of the nucleation mode peak ( $a_1$ ). The nucleation mode GMD becomes larger and the peak magnitude becomes smaller as the sample fraction and/or residence time increases because nucleated particles tend to coagulate with each other and form larger but fewer particles. This result is consistent with theory. Figure 5 shows the relationship between the nucleation peak magnitude and size. In the number domain, Figure 5 also shows that the magnitude decreases as the size increases.

Number concentrations can be translated to particle mass concentrations ( $m$ ) by assuming a uniform particle density,  $\rho$  ( $1 \text{ g/cm}^3$ ):

$$\frac{dm/d\log D_p}{C_{CO_2}} = (dN/d\log D_p) \frac{\pi}{6} \rho D_p^3$$

The mass distribution can also be fitted with a bi-modal log-normal function to get the mass-weighted mean diameter (MMD). Figure 5 includes the nucleation mode MMD and the mass domain peak magnitude at the MMD. Unlike in the number domain, the mass peak magnitude increases with the MMD and sample fraction. With higher sample fraction, the initial concentration of volatile materials is higher, so the gas-to-particle conversion rate

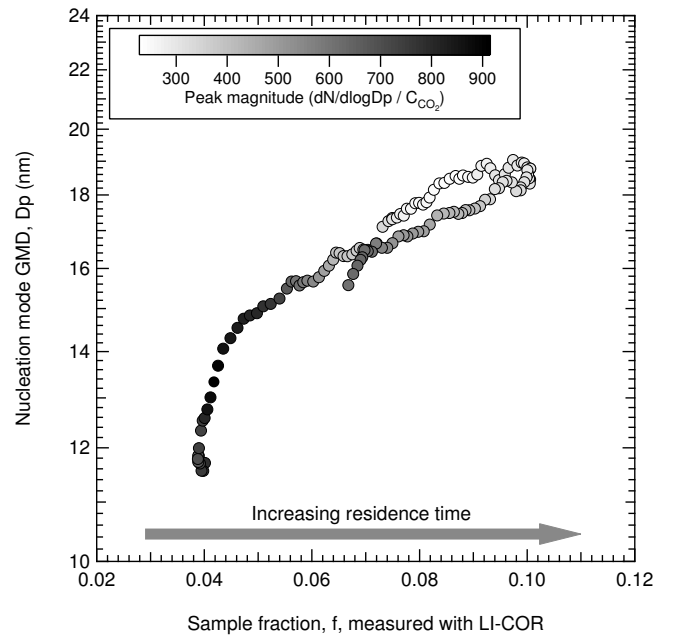


Figure 4. Nucleation mode geometric mean diameter (GMD) versus exhaust sample fraction.

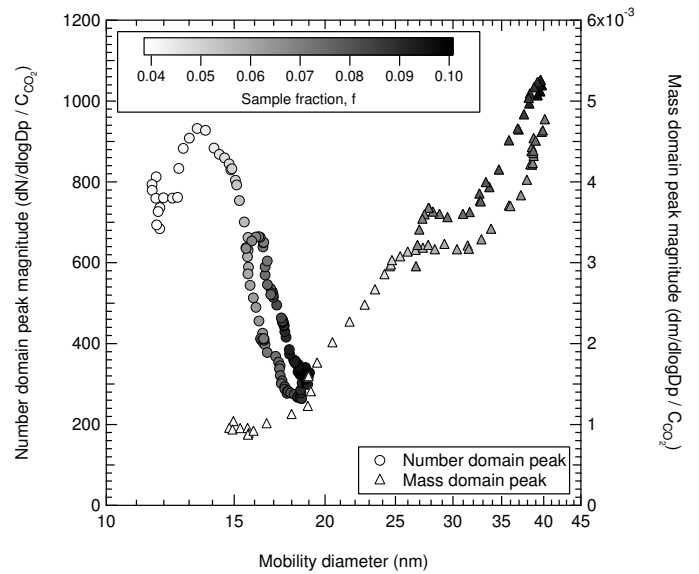


Figure 5. Nucleation mode peak magnitude versus mean diameters in the number (GMD) and mass (MMD) domains.

is faster. Moreover, the longer residence times associated with higher sample fractions allow even more volatiles to be converted to particle phase. Taken together, Figures 3-5 show that nucleation mode particles increase in size and total mass, but decrease in number, as residence time and/or sample fraction increases.

To verify the experimental result and better understand this complex microphysical processes, a numerical simulation was performed and shown in Figure 6. The model we used here has been briefly described in the Methods section, and Ref. [25] provides greater details including its mathematical formulations and some predictions. For this simulation, the geometric parameters and the flow configurations required by the algorithm were set to best represent the CE-5 experiment. Whereas the experimental

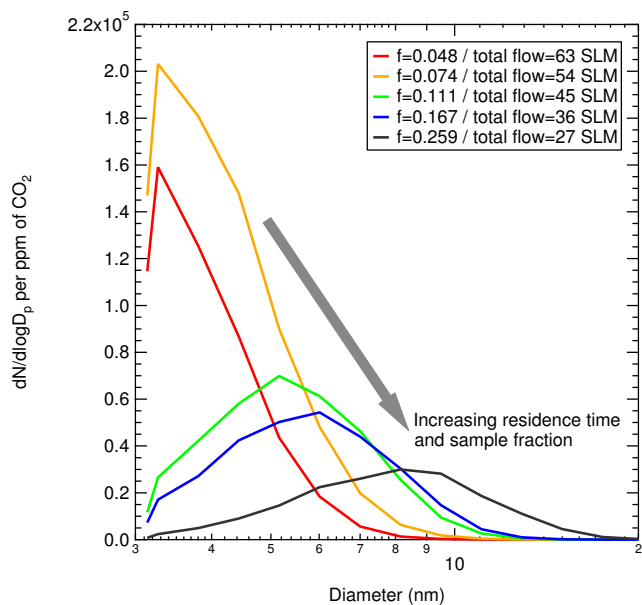


Figure 6. Microphysical simulation result of the nucleation particle size distribution representing the CE-5 test conditions (The monodisperse soot mode not shown).

data in Figure 3 contain both the nucleation and soot mode particles, Figure 6 only plots the nucleation mode particles from the simulation. Since the current version of the microphysical simulation code does not include the hydrocarbon microphysics, the simulation results may under-estimate the formation/growth of the particles; this is likely why the simulation results in Figure 6 show much higher number counts than the experimental data, but much smaller particle size, suggesting that the particles do not coagulate in the simulation as fast as in physical experiments. Nevertheless, the simulation results capture the trend well with respect to dilution rate. In both the experimental result (Figure 3) and the simulation result (Figure 6), the nucleation particle size grows and the number is reduced as the sample fraction ( $f$ ) is increased, and the total flow rate is decreased, *i.e.* residence time is increased. This is mainly because the longer residence time and higher sample fraction allow the nucleation particles to coagulate and form larger but fewer particles. In addition, longer residence time leads to more particle-to-wall loss in the transfer line (downstream of the dilution/aging chamber) and reduces the number of particles even further.

### On-Wing Aircraft Engine Test

Table 3 summarizes emissions index data obtained in the MDW-10 test using four different in-service CFM56-7 series engines operating at near idle power conditions. Previously published data from the CFM56-7 series engines during APEX-2 [15] are also included in the table for comparison. The table contains soot  $EI_m$  data (particulate mass produced per kilogram of fuel burnt) measured in MDW-10 and APEX-2 both using a conventional 1-m probe. Whereas idling CFM56-7 engines generated soot  $EI_m$  (mass-based emissions index) below 1 mg/kg-fuel during APEX-2, the  $EI_m$  measured during MDW-10 are higher than 30 mg/kg-fuel. In fact, the MDW-10  $EI_m$  data are comparable with the APEX-2 measurements for climb-out conditions ( $\sim 85\%$  thrust). We do not have a conclusive explanation for the

larger  $EI_m$ -soot values observed at MDW-10 than APEX-2, but we hypothesize that colder conditions at MDW-10 ( $\sim 265$  K) than APEX-2 ( $\sim 290$  K) may have modified combustor operation. Because of higher soot loading, and thus larger soot surface area, the volatile species are likely scavenged by the soot particles. In the SAEPA probe system, volatile PM precursors will form nucleation particles and increase the number concentration when the soot is present at low levels ( $< 10$  mg/kg-fuel). On the other hand, the volatile materials will condense on the soot particles and add mass without generating new particles if there is large enough soot surface area. This is consistent with what has been observed in downfield measurements when soot  $EI_m$  is high, e.g. APEX-2 high power conditions. APEX-2 data in Table 3 show that aged plumes ( $> 30$ -m measurements) produced at high power setting (high soot condition) generate almost an order of magnitude lower  $EI_n$  than from the same engine operating at idle power even while soot mass and number increase. The APEX-2 result implies that for  $EI_m > 10$  mg/kg-fuel, volatile species become coated on the soot rather than forming nucleation particles. The  $EI_m$  data are comparable for the idle MDW-10 and climb-out APEX-2 engines. Therefore, competition between nucleation and soot mode gas-to-particle process should be similar for these data sets despite the differences in operational power. The agreement between idle MDW-10  $EI_n$  and climb-out APEX-2  $EI_n$ , rather than idle, is consistent with current understanding of gas-to-particle conversion.

Also shown in Table 3 is particle-phase organic mass measured with the aerosol mass spectrometer (AMS). The APEX-2 data represent downfield measurements [15], and the MDW-10 data represent 1-m probe measurements using the SAEPA probe. The particle-phase organic was below detection capability of the AMS for the APEX-2 1-m probe. However, the SAEPA probe shows similar  $EI_m$ -organic as APEX-2 downfield measurement even though the sample was extracted at 1 m from the engine exit. Given that the engines were at idle and operating colder, the MDW-10 exhaust streams are expected to contain higher concentration of unburnt organic species than the APEX-2 climb-out exhaust. However, the MDW-10  $EI_m$ -organic data are not much higher than the APEX-2 climb-out conditions. We speculate that some hydrocarbon species might have been lost to the sampling line (before entering the dilution/aging chamber). Although not shown in Table 3, the AMS sulfate  $EI_m$  was somewhat low, too. To minimize gas-to-wall loss in the sampling line, the line temperature may need to be increased significantly higher than 150 °C. More rigorous lab testing is required to determine the optimal sampling line temperature.

In the case of MDW-10 engine #3, the SAEPA probe  $EI_n$  is noticeably higher than other engines, suggesting that larger number of nucleation particles were formed for this engine. The reason for the increased  $EI_n$  for engine #3 is likely the humid dilution gas ( $\sim 40\%$  relative humidity) used for engine #3. Figure 7 plots  $EI_n$  data obtained in MDW-10 via the SAEPA probe for dry and humid air, and clearly shows that the  $EI_n$  is increased with high humidity dilution. Sulfuric acid and water are two major species that drive the formation of nucleation particles [25, 46, 47]. Abundance of water molecules increases the sulfuric acid/water nucleation rate, and generates more particles [25]. The data show that dilution air humidity is an important variable to be considered.

Figure 8 shows the particle size distribution measured with the EEPS via the SAEPA probe during the MDW-10 campaign.

Table 3. EI comparison between MDW-10 and APEX-2 campaigns

Campaign	Engine model	Power	$EI_{m\text{-soot}}^a$ (mg/kg-fuel)	$EI_n (\times 10^{13} \text{ \#/kg-fuel})$		$EI_{m\text{-organic}}^c$ (mg/kg-fuel)
				Engine exit	Aged <sup>b</sup>	
MDW-10 (this work)	CFM56-7 #1	idle	<b>39 ± 15</b>		<b>110 ± 26</b>	0.31 ± 0.16
	CFM56-7 #2	idle	<b>46 ± 4.4</b>		<b>95 ± 39</b>	0.16 ± 0.11
	CFM56-7 #3 <sup>d</sup>	idle	<b>67 ± 17</b>		<b>534 ± 87</b>	0.82 ± 0.62
	CFM56-7 #4	idle	<b>31 ± 15</b>		<b>46 ± 6</b>	0.19 ± 0.09
APEX-2 (Ref. [15])	CFM56-7B22 #1	idle	<i>below detection</i>	2.5 ± 0.6	400 ± 200	0.3 ± 0.1
	CFM56-7B22 #2	climb-out	<b>80 ± 20</b>	16 ± 1	<b>53 ± 8</b>	0.5 ± 0.2
		idle	0.7 ± 0.5	2.7 ± 0.8	1400 ± 200	0.4 ± 0.1
		climb-out	<b>68 ± 8</b>	17 ± 1	<b>320 ± 10</b>	0.5 ± 0.05

<sup>a</sup> Conventional 1-m probe measurement with the MAAP both for MDW-10 and APEX-2

<sup>b</sup> CPC measurement via the SAEPA probe for MDW-10 and the >30-m probe for APEX-2

<sup>c</sup> 1-m measurement using the SAEPA probe for MDW-10 and >30-m measurement for APEX-2 (aged plume)

<sup>d</sup> For this engine, dilution air had about 40% relative humidity.

The EEPS data indicated that the nucleation mode is less pronounced at MDW-10 than CE-5. Figure 8 also shows that the nucleation peak magnitude becomes larger as the sample fraction is increased (indicated by higher CO<sub>2</sub> level) and the size does not change noticeably. This result may seem contrary to the CE-5 results where the nucleation particle size increased, and the peak magnitude decreased as the sample fraction was increased. Differences in the test setup are likely responsible for this apparent discrepancy. Whereas the sample fraction was coupled with the residence time during CE-5, we modified the system in MDW-10 so that the sample fraction could be varied without changing the residence time. In addition, we shortened the length of the final transfer line (between the dilution/aging chamber and mea-

surement equipment) in MDW-10 to 2 m compared to 15 m in CE-5. This prevented the newly formed nucleation/coagulation particles from being lost to the transfer line. A set of microphysical simulations similar to that performed for the CE-5 testing was performed to explain the MDW-10 results, and shown in Figure 9. In the MDW-10 simulation, the final transfer line was reduced to 2 m, and all other parameters were adjusted to best represent the MDW-10 test setup (see Table 1). Although the simulation results do not match the experimental results quantitatively, the trends are in good agreement; the peak magnitude increases as the sample fraction is increased, but the peak location does not change significantly. Unlike the CE-5 case, higher sample fraction did not lead

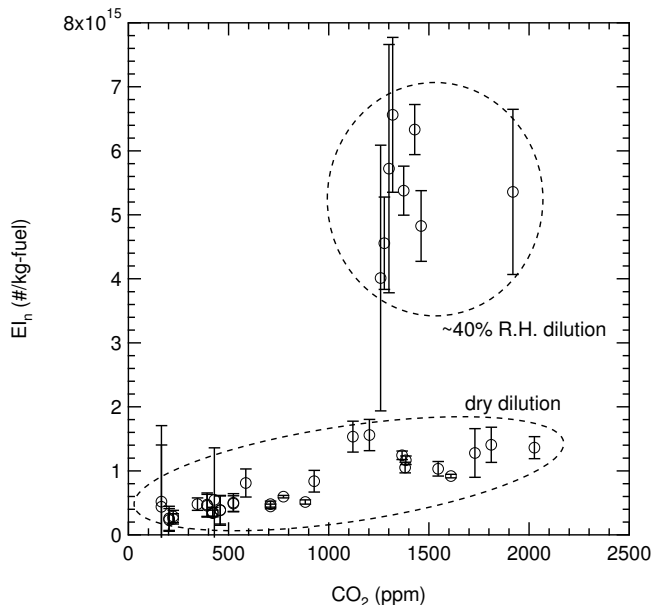


Figure 7. Impact of the water content in the dilution stream

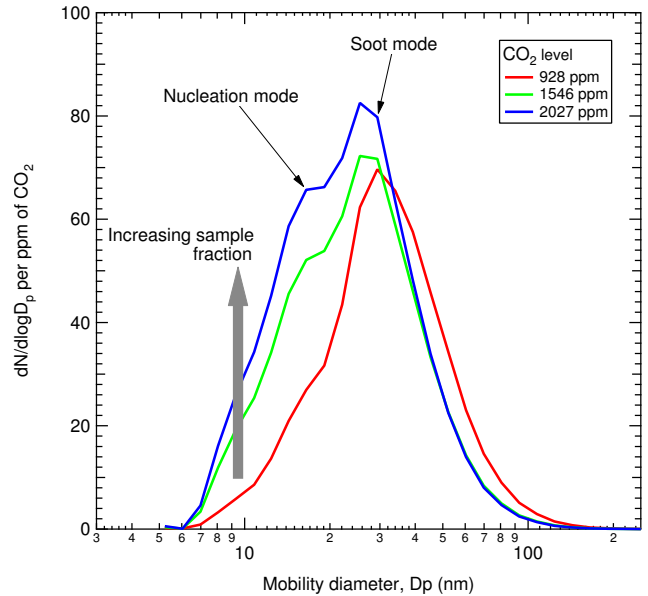


Figure 8. Particle size distribution (EPCS) obtained using the SAEPA probe during the MDW10 test. Higher CO<sub>2</sub> level indicates higher sample fraction ( $f$ )

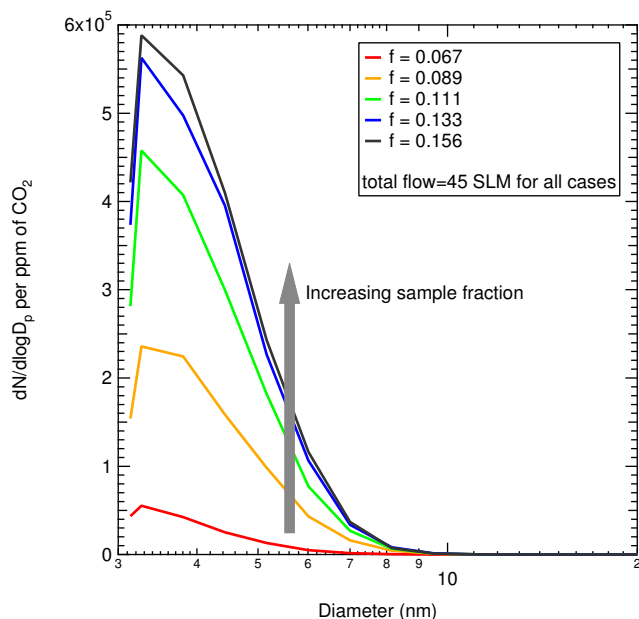


Figure 9. Microphysical simulation result of the nucleation particle size distribution representing the MDW-10 test conditions (The monodisperse soot mode not shown).

to the reduction of the peak magnitude in MDW-10 because 1) the final transfer line was very short, minimizing the effect of particle loss, and 2) we varied the sample fraction while keeping the total flow rate constant, eliminating the effect of residence time. These results suggest that to minimize the unwanted particle-to-wall loss, the location of the dilution/aging chamber needs to be planned carefully so that the transfer line lengths can be made as short as logistics and safety allow.

## CONCLUSION

We tested a sampling system that can condense volatile PM precursors to particle phase in a manner that is similar to what happens in the atmosphere. The instrument was deployed at the NASA Glenn Research Center and tested using a combustor rig. The SAEPA probe supported formation of both nucleation/growth mode particles and soot coatings as have been observed to form during atmospheric processing of jet engine exhaust. It was shown that nucleation mode particles increase in size and mass, but decrease in number, as residence time and/or sample fraction is increased. In the second deployment to Chicago Midway Airport, the SAEPA probe was tested using four separate on-wing, in-service CFM56-7 engines. Unlike conventional 1-m probe measurements of CFM56-7 engines, the SAEPA probe was able to promote formation of soot coatings as well as nucleation mode particles. Although the nucleation mode was weak due to dominant soot mode, the size and magnitude of nucleation particles depended on sample fraction as well as relative humidity of the dilution gas. The results from the field deployments are consistent with theoretical considerations, model predictions, and other field observations. The data and analysis make a strong point that the SAEPA probe system can be very useful in studying volatile particles in aircraft engine exhaust. For this reason, the approach has the potential to be adopted as a standard procedure for characterizing the volatile PM emissions from aircraft engines. We will seek

for future opportunities to deploy the system to additional field campaigns, and establish/refine general operating procedures optimized for specific purposes.

## ACKNOWLEDGMENT

This instrument development effort was supported by the Air Force SBIR program (contract number: FA9101-08-C-0013), and the authors are grateful to the support from Robert Howard, the AEDC SBIR technical monitor. NASA provided support for ARI participation in the CE-5 combustor testing through NRA contract number NNC07CB57C. The authors thank Kathy Tacina as well as the entire staff at NASA GRC for the support during the CE-5 test. We appreciate the ACRP 02-03a program for providing the opportunity to perform the MDW-10 measurements. Art Kaucher of Southwest Airlines, Matthew Marich and Aaron Frame of City of Chicago are greatly thanked for the cooperation and support during the MDW-10 measurements.

## NOMENCLATURE

$N$	Number concentration ( $\#/cm^3$ )
$m$	Mass concentration ( $\mu g/m^3$ )
$D_p$	Mobility diameter (nm)
$EL_m$	Mass-based emissions index (mg/kg-fuel)
$EL_n$	Number-based emissions index ( $\#/kg$ -fuel)
$f$	Sample fraction
$C_{CO_2}$	Volumetric concentration of $CO_2$ (ppm)
$\rho$	Density
GMD	Geometric mean diameter
MMD	Mass-weighted mean diameter
ppm	Parts per million
SLM	Standard ( $0^\circ C$ , 1 bar) liters per minute

## REFERENCES

- [1] Transportation Research Board, 2008, "Summarizing and Interpreting Aircraft Gaseous and Particulate Emissions Data," Airport Cooperative Research Program (ACRP) Report 9, www.TRB.org.
- [2] Unal, A., Hu, Y., Chang, M., Odman, M., and Russell, A., 2005, "Airport related emissions and impacts on air quality: Application to the Atlanta International Airport," *Atmospheric Environment*, **39**(32), pp. 5787–5798.
- [3] Lee, D., Fahey, D., Forster, P., Newton, P., Wit, R., Lim, L., Owen, B., and Sausen, R., 2009, "Aviation and global climate change in the 21st century," *Atmospheric Environment*, **43**(22-23), pp. 3520–3537.
- [4] Cho, S.-H., Yoo, J.-I., Turley, A., Miller, C., Linak, W., Wendt, J., Huggins, F., and Gilmour, M., 2009, "Relationships between composition and pulmonary toxicity of prototype particles from coal combustion and pyrolysis," *Proceedings of the Combustion Institute*, vol. 32, pp. 2717–2725.
- [5] Childers, J., Witherspoon, C., Smith, L., and Pleil, J., 2000, "Real-Time and Integrated Measurement of Potential Human Exposure to Particle-Bound Polycyclic Aromatic Hydrocarbons (PAHs) from Aircraft Exhaust," *Environmental Health Perspectives*, **108**(9), pp. 853–862.
- [6] Transportation Research Board, 2008, "Research Needs Associated with Particulate Emissions at Airports," Airport Cooperative Research Program (ACRP) Report 6, www.TRB.org.

- [7] Wong, H.-W., Yu, Z., Timko, M., Herndon, S., de la Rosa Blanco, E., Miake-Lye, R., and Howard, R., 2011, "Design Parameters for an Aircraft Engine Exit Plane Particle Sampling System," *Journal of Engineering for Gas Turbines and Power*, **133**(2), p. 021501.
- [8] Westerdaal, D., Fruin, S., Fine, P., and Sioutas, C., 2008, "The Los Angeles International Airport as a source of ultrafine particles and other pollutants to nearby communities," *Atmospheric Environment*, **42**, pp. 3143–3155.
- [9] Johnson, M., Hilton, M., Waterman, D., and Black, J., 2003, "Development of techniques to characterize particulates emitted from gas turbine exhausts," *Measurement Science and Technology*, **14**(7), pp. 1146–1150.
- [10] Wey, C., Anderson, B., Wey, C., Miake-Lye, R., Whitefield, P., and Howard, R., 2007, "Overview on the Aircraft Particle Emissions Experiment," *Journal of Propulsion and Power*, **23**(5), pp. 898–905.
- [11] Anderson, B., Cofer, W., Bagwell, D., Barrick, J., Hudgins, C., and Brunke, K., 1998, "Airborne observations of aircraft aerosol emissions I: Total nonvolatile particle emission indices," *Geophysical Research Letters*, **25**(10), pp. 1689–1692.
- [12] Anderson, B., Cofer, W., Barrick, J., Bagwell, D., and Hudgins, C., 1998, "Airborne observations of aircraft aerosol emissions II: Factors controlling volatile particle production," *Geophysical Research Letters*, **25**(10), pp. 1693–1696.
- [13] Wey, C., Anderson, B., Hudgins, C., Wey, C., Li-Jones, X., Winstead, E., Thornhill, L., Lobo, P., Hagen, D., Whitefield, P., Yelvington, P., Herndon, S., Onasch, T., Miake-Lye, R., Wormhoudt, J., Knighton, W., Howard, R., Bryant, D., Corporan, E., Moses, C., Holve, D., and Dodds, W., 2006, "Aircraft Particle Emission eXperiment (APEX)," Tech. Rep. NASA/TM-2006-214382, NASA.
- [14] Onasch, T., Jayne, J., Herndon, S., Worsnop, D., Miake-Lye, R., Mortimer, I., and Anderson, B., 2009, "Chemical Properties of Aircraft Engine Particulate Exhaust Emissions," *Journal of Propulsion and Power*, **25**(5), pp. 1121–1137.
- [15] Timko, M., Onasch, T., Northway, M., Jayne, J., Canagaratna, M., Herndon, S., Wood, E., Miake-Lye, R., and Knighton, W., 2010, "Gas Turbine Engine Emissions Part 2. Chemical Properties of Particulate Matter," *Journal of Gas Turbines and Power*, **132**.
- [16] Lobo, P., Hagen, D., Whitefield, P., and Alofs, D., 2007, "Physical Characterization of Aerosol Emissions from a Commercial Gas Turbine Engine," *Journal of Propulsion and Power*, **23**(5), pp. 919–929.
- [17] Cheng, M.-D., Corporan, D., DeWitt, M., Spicer, C., Holdren, M., Cowen, K., Laskin, A., Harris, D., Shores, R., Kagann, R., and Hashmonay, R., 2008, "Probing Emissions of Military Cargo Aircraft: Description of a Joint Field Measurement Strategic Environmental Research and Development Program," *Journal of the Air and Waste Management Association*, **58**, pp. 787–796.
- [18] Wey, T. and Liu, N.-S., 2007, "Modeling Jet Engine Aerosols in the Postcombustor Flow Path and Sampling System," *Journal of Propulsion and Power*, **23**(5), pp. 930–941.
- [19] Brundish, K., Clague, A., Wilson, C., Miake-Lye, R., Brown, R., Wormhoudt, J., Lukachko, S., Chobot, A., Yam, C., Waitz, I., Hagen, D., Schmid, O., and Whitefield, P., 2007, "Evolution of Carbonaceous Aerosol and Aerosol Precursor Emissions Through a Jet Engine," *Journal of Propulsion and Power*, **23**(5), pp. 959–970.
- [20] Petzold, A., Stein, C., Nyeki, S., Gysel, M., Weingartner, E., Baltensperger, U., Giebl, H., Hitzemberger, R., Döpelheuer, A., Vrchotický, S., Puxbaum, H., Johnson, M., Hurley, C., Marsh, R., and Wilson, C., 2003, "Properties of jet engine combustion particles during the PartEmis experiment: Microphysics and Chemistry," *Geophysical Research Letters*, **30**(13), p. 1719.
- [21] Herndon, S., Onasch, T., Frank, B., Marr, L., Jayne, J., Canagaratna, M., Grygas, J., Lanni, T., Anderson, B., Worsnop, D., and Miake-Lye, R., 2005, "Particle Emissions from In-use Commercial Aircraft," *Aerosol Science and Technology*, **39**(8), pp. 799–809.
- [22] Herndon, S., Jayne, J., Lobo, P., Onasch, T., Fleming, G., Hagen, D., Whitefield, P., and Miake-Lye, R., 2008, "Commercial Aircraft Engine Emissions Characterization of in-Use Aircraft at Hartsfield-Jackson Atlanta International Airport," *Environmental Science and Technology*, **42**(6), pp. 1877–1883.
- [23] Johnson, G., Mazaheri, M., Ristovski, Z., and Morawska, L., 2008, "A Plume Capture Technique for the Remote Characterization of Aircraft Engine Emissions," *Environmental Science and Technology*, **42**(13), pp. 4850–4856.
- [24] Mazaheri, M., Johnson, G., and Morawska, L., 2009, "Particle and Gaseous Emissions from Commercial Aircraft at Each Stage of the Landing and Takeoff Cycle," *Environmental Science and Technology*, **43**(2), pp. 441–446.
- [25] Wong, H.-W., Yelvington, P., Timko, M., Onasch, T., and Miake-Lye, R., 2008, "Microphysical Modeling of Ground-Level Aircraft-Emitted Aerosol Formation: Roles of Sulfur-Containing Species," *Journal of Propulsion and Power*, **24**, pp. 590–602.
- [26] Romay, F., Takagaki, S., Pui, D., and Liu, B., 1998, "Thermophoretic Deposition of Aerosol Particles in Turbulent Pipe Flow," *Journal of Aerosol Science*, **29**(8), pp. 943–959.
- [27] Friedlander, S., 2000, *Smoke, Dust and Haze*, John Wiley and Sons, New York, NY.
- [28] Tsai, C.-J., Lin, J.-S., Aggarwal, S., and Chen, D., 2004, "Thermophoretic Deposition of Particles in Laminar and Turbulent Tube Flows," *Aerosol Science and Technology*, **38**(2), pp. 131–139.
- [29] Nickels, T. and Perry, A., 1996, "An Experimental and Theoretical Study of the Turbulent Coflowing Jet," *Journal of Fluid Mechanics*, **309**, pp. 157–182.
- [30] Davidson, M. and Wang, H., 2002, "Strongly Advected Jet in a Coflow," *Journal of Hydraulic Engineering*, **128**(8), pp. 742–752.
- [31] Jayne, J., Leard, D., Zhang, X., Davidovits, P., Smith, K., Kolb, C., and Worsnop, D., 2000, "Development of an Aerosol Mass Spectrometer for Size and Composition Analysis of Submicro Particles," *Aerosol Science and Technology*, **33**, pp. 49–70.
- [32] Petzold, A. and Schoönlinner, K., 2004, "Multi-angle absorption photometry - a new method for the measurement of aerosol light absorption and atmospheric black carbon," *Aerosol Science and Technology*, **35**, pp. 421–441.
- [33] Sem, G. J., 2002, "Design and performance characteristics of three continuous-flow condensation particle counters: a summary," *Atmospheric Research*, **62**(3-4), pp. 267–294.
- [34] Hagen, D., Lobo, P., Whitefield, P., Trueblood, M., Alofs, D., and Schmid, O., 2009, "Performance Evaluation of a Fast Mobility-Based Particle Spectrometer for Aircraft Exhaust," *Journal of Propulsion and Power*, **25**(3), pp. 628–634.
- [35] Tacina, R., Wey, C., Laing, P., and Mansour, A., 2002, "A Low NOx Lean-Direct Injection, Multipoint Integrated Module Combustor Concept for Advanced Aircraft Gas Turbines," Tech. Rep. NASA/TM-2002-211347, NASA.
- [36] Bergmann, M., Kirchner, U., Vogt, R., and Benter, T., 2009, "On-road and laboratory investigation of low-level pm emissions of a modern diesel particulate filter equipped diesel passenger car," *Atmospheric Environment*, **43**, pp. 1908–1916.
- [37] Price, P., Stone, R., Collier, T., Davies, M., and Scheer, V., 2006, "Dynamic Particulate Measurements from a DISI Vehicle: A Comparison of DMS500, ELPI, CPC and PASS," SAE Technical Paper Series 2006-01-1077, SAE International.
- [38] Zervas, E. and Dorlhéne, P., 2006, "Comparison of Exhaust Particle Number Measured by EEPS, CPC, and ELPI," *Aerosol Science and Technology*, **40**, pp. 977–984.
- [39] Agrawal, H., Sawant, A., Jansen, K., Miller, J., and Cocker III, D., 2008, "Characterization of chemical and particulate emissions from aircraft engines," *Atmospheric Environment*, **42**, pp. 4380–4392.

- [40] Kärcher, B., Yu, F., Schröder, F., and Turco, R., 1998, "Ultrafine aerosol particles in aircraft plumes: Analysis of growth mechanisms," *Geophysical Research Letters*, **25**(15), pp. 2793–2796.
- [41] Schröder, F., Brock, C., Baumann, R., Petzold, A., Busen, R., Schulte, P., and Fiebig, M., 2000, "In situ studies on volatile jet exhaust particle emissions: Impact of fuel sulfur content and environmental conditions on nuclei mode aerosols," *Journal of Geophysical Research*, **105**(D15), pp. 19,941–19,954.
- [42] Yelvington, P., Herndon, S., Wormhoudt, J., Jayne, J., Miake-Lye, R., Knighton, W., and Wey, C., 2007, "Chemical Speciation of Hydrocarbon Emissions from a Commercial Aircraft Engine," *Journal of Propulsion and Power*, **23**(5), pp. 912–918.
- [43] Knighton, W., Rogers, T., Anderson, B., Herndon, S., Yelvington, P., and Miake-Lye, R., 2007, "Quantification of Aircraft Engine Hydrocarbon Emissions Using Proton Transfer Reaction Mass Spectrometry," *Journal of Propulsion and Power*, **23**(5), pp. 949–958.
- [44] Kurzke, J., 2004, *GasTurb10: A Program for Gas-Turbine Performance Calculations*.
- [45] Timko, M., Yu, Z., Onasch, T., Wong, H.-W., Miake-Lye, R., Beyersdorf, A., Anderson, B., Thornhill, K., Winstead, E., Corporan, E., DeWitt, M., Klingshirm, C., Wey, C., Tacina, K., Liscinsky, D., Howard, R., and Bhargawa, A., 2010, "Particulate Emissions of Gas Turbine Engine Combustion of a Fischer-Tropsch Synthetic Fuel," to appear in *Energy and Fuels*.
- [46] Yu, F., 2005, "Quasi-Unary Homogeneous Nucleation of  $\text{H}_2\text{SO}_4\text{-H}_2\text{O}$ ," *Journal of Chemical Physics*, **122**(7), pp. 074501/1–074501/8.
- [47] Yu, F., 2007, "Improved Quasi-Unary Nucleation Model for Binary  $\text{H}_2\text{SO}_4\text{-H}_2\text{O}$  Homogeneous Nucleation," *Journal of Chemical Physics*, **127**(5), pp. 054301/1–054301/8.